OFFPRINTS FROM NEW CHARACTERIZATION TECHNIQUES FOR THIN POLYMER FILMS
Edited by Hsu-Ming Tong and Luu T. Nguyen
Copyright (c) 1990 by John Wiley & Sons, Inc.

13
ADHESION MEASUREMENT OF THIN POLYMER FILMS BY INDENTATION

M. J. Matthewson*

Almaden Research Center
IBM Research Division
San Jose, California

J. E. Ritter

Mechanical Engineering Department
University of Massachusetts at Amherst
Amherst, Massachusetts

13.1 INTRODUCTION

The adhesion of thin polymer films is usually crucial to their successful performance. Despite its importance, adhesion is difficult to quantify in a physically meaningful way. While there is an extensive literature on thin film adhesion (for example, Ref. 1 presents a selected bibliography of over 300 references), no entirely satisfactory test method has yet emerged. This chapter describes the indentation technique which has recently been developed for thin film adhesion measurement. This technique is unique in being able to determine in one experiment the two adhesion parameters required to uniquely specify interfacial strength. The technique, while applied here to adhesion of polymer films, is generally applicable to other film materials.

Any adhesion test requires that the interface between the thin film and the substrate be subjected to stress (usually shear but sometimes normal tension or a combination of the two) sufficiently large to cause failure. The indentation technique, shown schematically in Fig. 13.1 for the case of a ball indenter, is a particularly simple and convenient method for applying an in-plane stress to the film. The indenter is loaded normally onto the film, typically using an Instron machine, which deforms and displaces laterally. This lateral motion of the film results in a shear stress across the interface which, at sufficiently high indenter loads, causes an interfacial crack to initiate and subsequently propagate. The crack is readily observed if a transparent substrate is used. If the crack is not visible by direct observation it may be detected by ultrasonic imaging or acoustic emission. While as yet no measurements have been made on films thinner than about 10 μm there is no reason in principal why very much thinner films can not be used, providing that the debond crack is still visible.

---

* Present address: Fiber Optic Materials Research Program, Rutgers University, P.O. Box 909, Piscataway, New Jersey 08855.

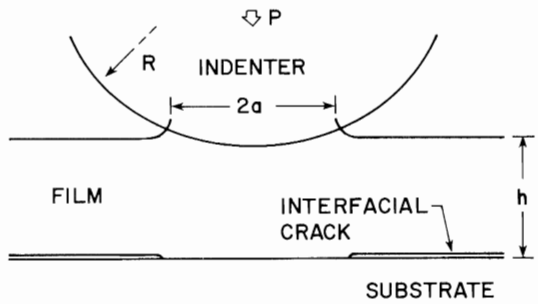

Figure 13.1: Schematic diagram of the indentation test for adhesion measurement. The indenter (a sphere here) is loaded onto the film until a crack forms in the interface.

It is frequently overlooked that interfacial strength needs to be specified by two independent parameters. The first, usually called the interfacial fracture resistance, is analogous to the fracture toughness of a bulk solid and is a measure of the energy required to create a unit area of interfacial crack. The interfacial fracture resistance is normally measured by determining the stress or load required to extend an interfacial crack of known geometry. The resistance is then calculated from energy balance considerations. The second parameter is a strength parameter which depends on the fracture resistance and strength-controlling defects as well as on the nature of the strength measurement technique (shear, tension, etc.) and on any residual deposition stresses in the film. The importance of knowing both adhesion parameters may be illustrated with the following example. If an interface is found to be unacceptably weak then this could be caused by either having an inherently weak interface because of poor bonding (i.e., low fracture resistance), or by having large interfacial defects. These two possible problems would be solved by different techniques so the exact cause of the weakness needs to be known, but can not be determined by either a strength or fracture resistance measurement alone.

The indentation technique is unique in its ability to measure both adhesion parameters in one experiment. The indenter is loaded onto the film until a critical load is reached where fracture initiates; further loading causes the interfacial crack to grow stably. Thus, this test is able to examine both the initiation and propagation stages of fracture. In contrast, other test techniques look only at one stage. For example, the "pin pull" test (in which a pin is glued to the thin film and then pulled off) examines initiation only since pull-off represents the onset of catastrophic failure. On the other hand, the "peel" test examines the stable propagation of an interfacial crack. Thus, these two tests measure quite different parameters since the initiation stage is determined by the strength of the interface while the propagation stage is determined by the interfacial fracture resistance.

Although the indentation technique is in its infancy and much work remains to be done before it is fully understood, particularly in the analysis of the propagation stage, substantial understanding of the failure mechanisms has been achieved and we will now describe how the indentation test can be used to measure interfacial failure.

13.2 THE INITIATION STAGE OF FAILURE

Matthewson (2) and Ritter et al. (3) studied the adhesion of a range of thin polymeric films on rigid substrates using the indentation technique and found that, even though the details of the film deformation were quite variable, the adhesive failure initiated in essentially the same way for all systems studied. For example, Fig. 13.2 [from Ritter et al. (3)] shows a typical sequence of micrographs of the indenter/film contact zone viewed through the substrate for a 4-mm-diameter sphere indenting a 98-μm-thick epoxy film on a glass substrate. As the indenter load is increased, a debond crack initiates close to the contact edge at some quite well-defined load (at about 40 N in this case, Fig. 13.2c) and grows around the edge of the contact and extends radially outwards; it does not extend far into the contact region because of the high compressive stress across the film/substrate interface in this region. Further loading extends the debond crack, though in the case shown in Fig. 13.2, it is not exactly circular due to local fluctuations in adhesive strength. The debonded zone does not extend further on unloading and is still visible under zero indentation load (Fig. 13.2f).

The stress field acting across the film/substrate interface at the debond crack initiation position, at or near the contact edge, is approximately pure radial shear since there is negligible normal stress across the interface at this position. Matthewson (2) proposed a shear stress failure criterion for the polyester/abraded glass system he studied, which predicts that the failure initiates when the interfacial shear stress at the contact edge exceeds some critical value, τ_c. Ritter et al. (3) showed that this criterion was applicable to a range of film materials with different mechanical properties and adhesions. It is necessary to calculate the interfacial shear strength, τ_c, from measurements of the critical load to initiate debonding, P_c, and the contact geometry at debonding but the exact relationship depends on the type of deformation of the film beneath the indenter which may range from fully elastic to predominantly plastic. Ritter (3) identified three distinct types of behavior, shown schematically in Fig. 13.3, which are distinguished by differing deformation mechanisms of the film and substrate, though the debonding mechanism is the same for all three. Type I occurs when the deformation of the film remains elastic up until debonding occurs; in Type II the film deformation is predominantly plastic or irreversible at debonding but the film is not penetrated and Type III occurs when the indenter has penetrated the film before debonding occurs so that some indentation load is supported directly by the substrate. The failure type for a given system will depend on the film thickness and adhesion and the indenter sharpness. Blunt indenters and thick, poorly adhering films favor Types I and II while sharp indenters or thin, well-adhering films favor Types II and III. Between these types are regions of mixed behavior, particularly between Types I and II, where the film deformation is elastoplastic. Analysis of these regions is difficult so they should be avoided by suitable choice of indenter profile or sharpness. Pointed indenters, such as the Vickers pyramid indenter, are infinitely sharp and produce plastic deformation and can be used to produce Type II or Type III debonding. Elastic deformation, and hence Type I debonding, can be produced by employing sufficiently large radius spherical indenters. However, a small amount of plastic deformation may significantly perturb the elastic stress field under the indenter but may conveniently be detected by measuring the contact radius as a function of indenter load on both the loading and unloading cycle. Any discrep-

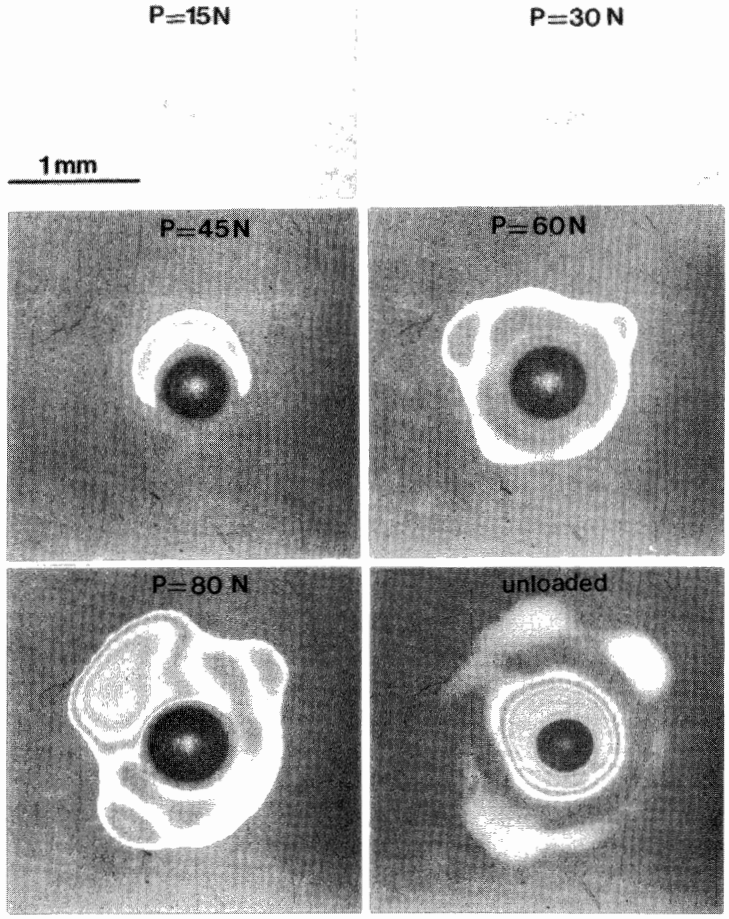

Figure 13.2: Sequence of optical micrographs showing debonding of 98-μm epoxy film on a glass substrate with increasing indenter load. (a) 15 N, (b) 30 N, (c) 45 N, (d) 60 N, (e) 80 N and (f) after unloading. From Ritter et al. (3).

ancy between the two sets of measurements, particularly at low load, is indicative of plastic deformation that may not be readily apparent by visual inspection for residual deformation. Some preliminary experimentation is usually necessary to ensure a pure type. The three types will now be described in more detail and the corresponding equations will be given which enable the interfacial shear strength to be determined from the critical debonding load.

13.2.1 Type I - Elastic Film Deformation

Ritter et al. (3) have considered debonding under conditions of elastic deformation of the film when indented by a sphere. Figure 13.1 is a schematic showing the geometry of the contact. In principal any indenter shape that results in elastic deformation

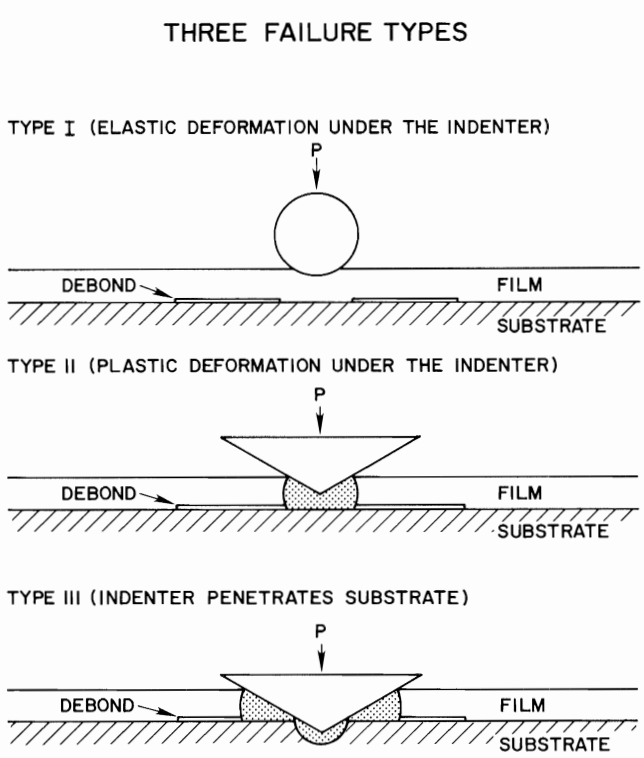

Figure 13.3: Schematic diagram of the three types of debonding.

could be used but spheres are readily available and their contact mechanics have been widely studied. The interfacial shear stress is a maximum inside the contact zone, typically at $r \sim 0.8a$. The large compressive normal stress across the interface inhibits interfacial failure (e.g., Ref. 4) so that failure initiates near the edge of the contact where the normal stress is zero. This has been observed experimentally by Ritter et al. (3). There are many analyses available for the elastic contact of a sphere on a thin compliant film attached to a rigid substrate (q.v., Ref. 5) the majority being numerical in nature and hence difficult to use. However, Ritter et al. (2) used an analysis due to Matthewson (6) which, though approximate since it is asymptotically correct for thin films, is unique in yielding results that are analytic and expressible in closed form. This makes the analysis of experimental data particularly simple compared with using more accurate treatments requiring complex numerical calculations. The error in Matthewson's analysis is typically a few percent which is not significant compared to the experimental error in the indentation technique. There exists a discontinuity in the interfacial shear stress at the contact edge, $r = a$, due to the approximate nature of the analysis, but a value for the shear stress, τ_i, averaged across the discontinuity, is given by

$$\tau_i = G\left[\frac{\alpha}{2}K_1\left(\frac{\phi a}{h}\right) + \frac{\nu a}{(1-2\nu)R} - \frac{\beta}{2}I_1\left(\frac{\gamma a}{h}\right)\right], \quad \nu < \frac{1}{2} \tag{1a}$$

$$\tau_i = G\left[\frac{17a^3}{24h^2R}\frac{K_1\left(\frac{\phi a}{h}\right)}{K_1\left(\frac{\phi a}{h}\right) - \frac{\phi a}{h}K'_1\left(\frac{\phi a}{h}\right)} + \frac{a}{4R}\right], \quad \nu = \frac{1}{2} \tag{1b}$$

where G and ν are the shear modulus and Poisson's ratio for the film, h is the film thickness, R is the indenter radius, and

$$\phi = \sqrt{\frac{6(1-\nu)}{4+\nu}}$$

$$\gamma = \sqrt{\frac{3(1-2\nu)}{2(1-\nu)}}$$

$$\beta = \frac{\left[\frac{\phi a}{h}K'_1\left(\frac{\phi a}{h}\right) - K_1\left(\frac{\phi a}{h}\right)\right]\left(\frac{h}{2R}\right)(1-6\nu)}{\left[\gamma K_1\left(\frac{\phi a}{h}\right)I'_1\left(\frac{\gamma a}{h}\right) - \phi I_1\left(\frac{\gamma a}{h}\right)K'_1\left(\frac{\phi a}{h}\right)\right](1-2\nu)}$$

$$\alpha = \frac{-4}{(4+\nu)\phi K'_1\left(\frac{\phi a}{h}\right)}\left[\frac{(1-6\nu)h}{2R(1-2\nu)} + \beta\gamma I'_1\left(\frac{\gamma a}{h}\right)\right]$$

with $I_i(x)$ and $K_i(x)$ being the ith order (i = 0, 1, . . .) modified Bessel functions of the first and second kind and $I'_i(x)$ and $K'_i(x)$ are their derivatives:

$$I'_1(x) = \frac{d}{dx}I_1(x) = \frac{1}{2}[I_0(x) + I_2(x)]$$

$$K'_1(x) = \frac{d}{dx}K_1(x) = -\frac{1}{2}[K_0(x) + K_2(x)]$$

The indenter load, P, and the contact radius, a , are related by

$$P = \pi a^2 G\left[\frac{2\nu h(1-6\nu)}{3R(1-2\nu)^2} + \frac{4\nu\beta h}{3a(1-2\nu)}I_1\left(\frac{\gamma a}{h}\right) + \frac{2(1-\nu)}{1-2\nu}\left(\frac{a^2}{4Rh} - \delta\right)\right], \quad \nu < \tfrac{1}{2} \tag{2a}$$

$$P = \pi a^2 G\left[\frac{a^4}{32h^3R}\left(\frac{6K_1\left(\frac{\phi a}{h}\right)}{K_1\left(\frac{\phi a}{h}\right) - \frac{\phi a}{h}K'_1\left(\frac{\phi a}{h}\right)} + 1\right) + \frac{9a^2}{8hR}\right], \quad \nu = \frac{1}{2} \tag{2b}$$

where

$$\delta = -\frac{\nu(4+\nu)h\alpha}{12a(1-\nu)}\left[\frac{\phi a}{h}K'_1\left(\frac{\phi a}{h}\right) + K_1\left(\frac{\phi a}{h}\right)\right]$$

Equations (1) and (2) may be combined to eliminate G to give the critical interfacial shear stress, τ_c, in terms of the critical debonding load, P_c, the contact radius at that load a_c, and the other variables. τ_c is of the form:

$$\tau_c = \frac{P_c}{\pi a_c^2} f\left(\frac{a_c}{h}, \nu\right) \tag{3}$$

Figure 13.4 shows the dimensionless quantity $\tau_c \pi a_c^2/P_c$ as a function of a_c/h for various values of ν. Each line is a universal curve for that value of ν. (Note that both τ_c and P_c are inversely proportional to R so that R dependence cancels.) h and R are readily measured; ν can be measured or estimated but it should be noted that Eqs. (1) and (2) are extremely sensitive to ν as ν approaches ½. This is not apparent from Fig. 13.4 because of the normalization to P_c which is also sensitive to ν. For example, Fig. 13.5 shows the variation of interfacial stress at the contact edge [Eq. (1)] as a function of the film Poisson's ratio, ν, calculated for $a/h = 5$. (The shear stress is normalized by the factor R/Ga in order to remove G and R dependence.) Therefore, ν needs to be known accurately for elastomers and other high Poisson's ratio materials. a_c can either be measured during the indentation experiment at the same time as P_c or it can be deduced from Eq. (2) in which case the shear modulus of the film, G, also requires measurement. The shear modulus of the film may be measured in various ways; Matthewson (6) detached strips of film and directly measured extension of the film as a function of applied load. Alternatively, if ν is known the shear modulus can be determined in situ by measurements of the contact radius as a function of indenter load using Eq. (2). For example, Fig. 13.6 shows load and contact radius data from Matthewson (6) for a 47-mm-radius sphere contacting a 2.15-mm thick rubber ($\nu = 0.5$) film. The theory line, calculated for a film shear modulus of 89 kPa, shows excellent agreement with the data.

The indenter radius should be chosen judiciously for either adhesion or modulus measurements. Equations (1) and (2) are only accurate for asymptotically thin films and so for better than 10% accuracy $a/h > 2$. Also, the maximum strain in the film, which is in the normal direction (z) and at the contact center, should not be large, that is, $\varepsilon_z < 20$ where

$$\varepsilon_z = -\frac{a^2}{2Rh} + \delta$$

These constraints define a region in the (a/h, r/h) plane bounded by $a/h = 2$ and $\varepsilon_z = 0.2$ for which the stress analysis is accurate. This region is shown in Fig. 13.7 for two representative values of the film Poisson's ratio (a) $\nu = 0.5$ and (b) $\nu = 0.35$. For modulus determinations an indenter as large as is practicable should be used since then Eq. (2) is valid over the largest range of contact radius, a. Also shown dashed in Fig. 13.7 are loci for various adhesive strengths, $\tau_c/G = 0.01$, 0.02, and 0.05. For a particular film system an indenter radius for adhesion determination should be chosen that corresponds to a section of the τ_c/G locus which lies within the

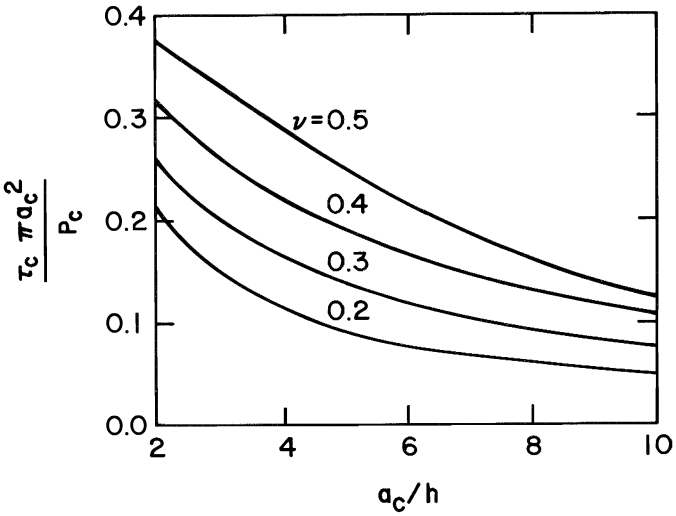

Figure 13.4: Universal curves of the dimensionless interfacial shear strength for various values of ν.

region of accuracy. For higher Poisson's ratio films (e.g., Fig. 13.7a) a large indenter radius should be chosen, while for lower Poisson's ratio films with good adhesion (e.g., Fig. 13.7b) a smaller radius might be necessary since the τ_c/G locus crosses both boundaries of the region of accuracy leaving only a limited range of indenter radii for which the stress analysis is accurate.

To summarize, the interfacial shear strength, τ_c, may be estimated from straightforward measurements of P_c and a_c using Eqs. (1) and (2). This represents a major advantage of the indentation technique over other methods since all the important mechanical parameters of the film can be measured during the adhesion test. Not only is this very convenient but in a typical experiment the film system may be subjected to an environment which degrades the adhesion. Such an environment is also likely to alter the mechanical properties of the film but any such change is automatically taken into account by the indentation technique; thus, the test can be used to determine the effects of environment on adhesion.

In practice it is usually difficult to apply a thin film that is stress-free so that the effect of residual deposition stresses on the indentation experiment need to be understood. Ritter et al. (3) point out that, by the principal of superposition, a uniform residual stress has no effect on the interfacial shear stress throughout elastic deformation so that the measured adhesive shear strength is predicted to be independent of residual stress in the film for Type I debonding.

13.2.2 Type II - Plastic Deformation without Penetration

Matthewson (2) studied the case of predominantly plastic deformation of the coating beneath the indenter and made measurements of the critical load for debonding and the corresponding contact radius, for various film thicknesses and spherical indenter

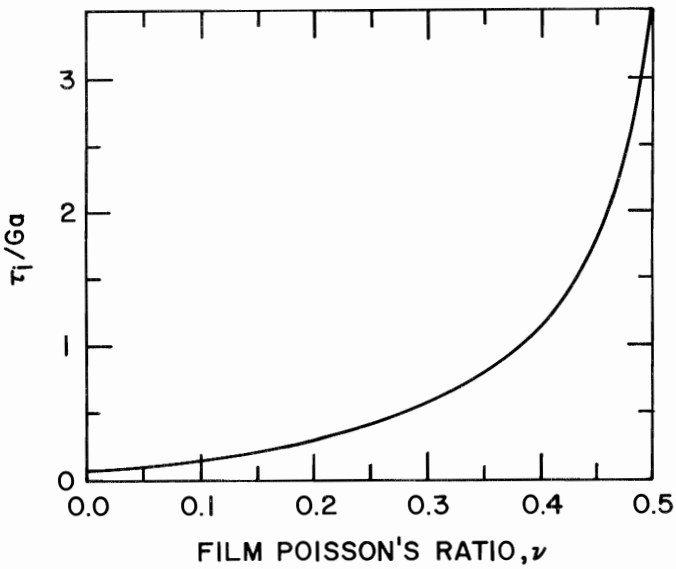

Figure 13.5: Variation of the normalized interfacial shear stress at the contact edge, $\tau_i R/Ga$, with film Poisson's ratio, ν, calculated from Eq. (1) using $a/h = 5$.

radii. He proposed a model for this system (Fig. 13.8) in which the plastic zone, assumed to be a cylinder of radius a, is replaced by a pressurized hole applying a radial stress, σ_r, to the surrounding elastically deforming film. Assuming no work hardening and the Tresca yield criterion, σ_r is given by

$$\sigma_r = Y - H \tag{4}$$

where Y is the compressive yield strength of the film material and H is the mean contact pressure, $P/\pi a^2$, which can be taken to be the hardness of the film. Matthewson assumed that $H \sim 3Y$ but Ritter et al. (3) pointed out that $H \sim 2.25Y$ is more appropriate for polymeric film materials (7), the former expression being more appropriate for metal films. The latter expression gives $\sigma_r = -0.56H$ which Matthewson then uses as a boundary condition at $r = a$ for the elastic solution for stresses outside the contact region (6). The interfacial shear stress is a maximum at the boundary $r = a$, and, denoting values of parameters at the critical point for debonding by the subscript c, the interfacial shear strength is given by

$$\tau_c = \frac{-0.56H_c}{\dfrac{K'_1\left(\dfrac{\phi a_c}{h}\right)}{\phi K_1\left(\dfrac{\phi a_c}{h}\right)} + \dfrac{\nu h}{a_c \phi^2}} \tag{5}$$

where

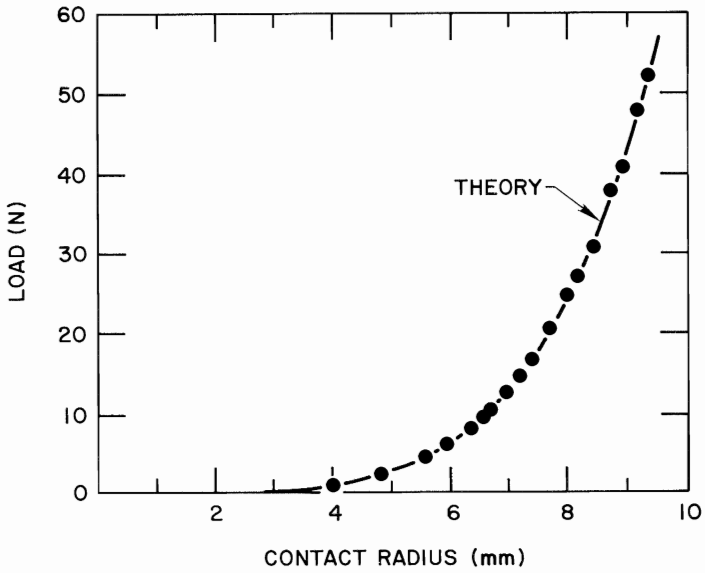

Figure 13.6: Measurements of load and contact radius for indentation of a 2.15-mm-film of rubber ($\nu = 0.5$) by a 47-mm-radius sphere. The theory line is calculated from Eq. (2) using G = 89 kPa (after Ref. 6).

$$H_c = \frac{P_c}{\pi a_c^2} \tag{6a}$$

or for a Vickers pyramid indenter

$$H_c = \frac{P_c}{2b_c^2} \tag{6b}$$

where b_c is half the diagonal length of the film/indenter contact area. Equations (5) and (6a) give that τ_c for a ball indenter is of the form

$$\tau_c = H_c \cdot f\left(\frac{a_c}{h}, \nu\right) \tag{7}$$

The hardness, H_c, is determined from the indenter load and contact radius (or diagonal) at debonding. In general, H_c can depend on the film thickness and in such cases will be higher than the hardness of bulk film material due to the confinement by the rigid substrate. However, provided a_c is not too much greater than h, then H_c can be taken to be approximately independent of h. Given that τ_c and ν are expected to be independent of h, then Eq. (7) predicts that the aspect ratio of the plastic zone, a_c/h, is a constant at debonding so that Eq. (6a) predicts that P_c/h^2 is a constant. Matthewson's adhesion test data for polyester films on abraded glass substrates do indeed show a parabolic relationship between critical stress for debonding and film

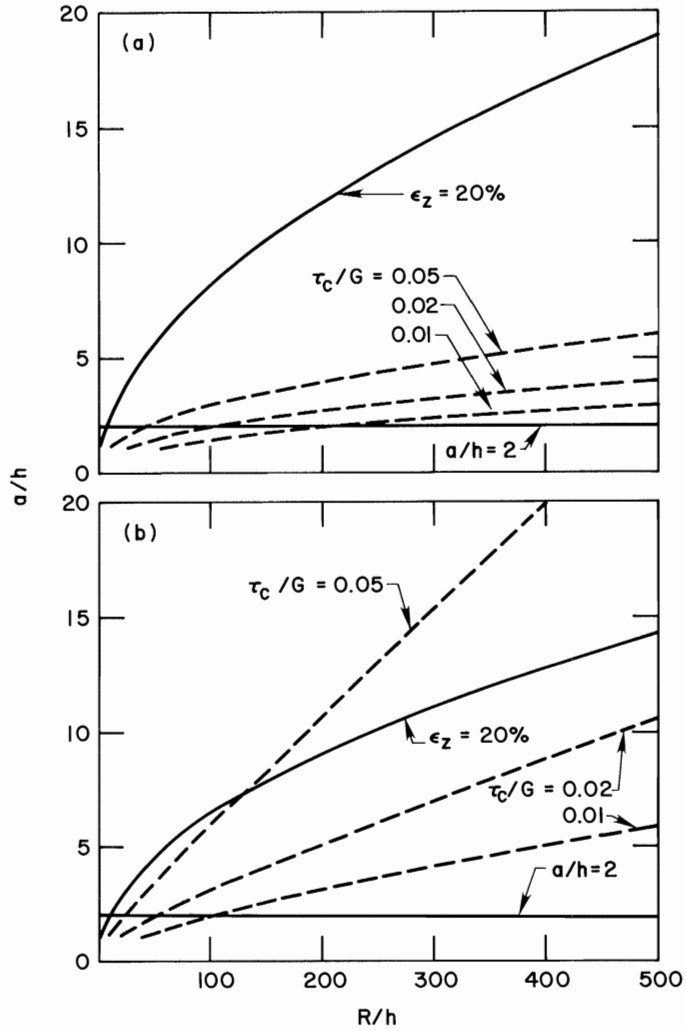

Figure 13.7: Region of accuracy for the contact stress solutions for an elastic film on a rigid substrate indented by a sphere; calculated for film Poisson's ratio (a) $\nu = 0.5$ and (b) $\nu = 0.35$.

thickness. For example, Fig. 13.9 shows data for indentation by a 4-mm-diameter sphere on polyester films of various thicknesses in the 100- to 1000-μm range on abraded glass substrates. Again, like Type I debonding, all important mechanical properties of the film (its hardness) are measured during the indentation experiment; necessarily providing values that are appropriate for the indentation conditions and film thickness.

It should be noted that Eq. (5) does not explicitly contain the indenter radius, R. In fact the indenter profile is not relevant to the analysis since it is effectively masked

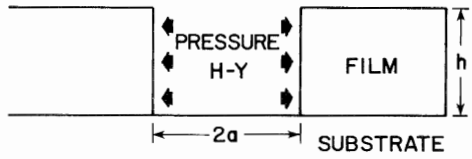

Figure 13.8: Schematic diagram of the model for Type II debonding (after Ref. 2).

by the plastic zone in the film. A nonaxisymmetric indenter, such as the Vickers pyramid, could even be used without loss of accuracy.

In contrast to Type I debonding, a uniform residual stress in the film, σ_{res}, does affect the interfacial shear stress for Type II debonding; in this case, the numerator of Eq. (5) is offset by the residual stress and should be replaced by $-(0.56H_c + \sigma_{res})$ (2). A uniform tensile residual stress in the film reduces the critical load for debonding since the residual stress also contributes to the net interfacial shear stress. Ritter et al. (3) suggest this difference between Types I and II may be used to measure the residual stress since any difference in interfacial shear strength measured under Type II conditions, compared to Type I conditions, must be due to the residual stress which can then be estimated by the modified form of Eq. (5).

13.2.3 Type III - Plastic Deformation with Penetration

When the film is penetrated at debonding, the substrate supports a portion of the applied indenter load as shown in Fig. 13.10 for a Vickers indenter. The interfacial shear strength can still be determined using Eq. (5) but H_c should be replaced by H_c^f, the film hardness, and a_c replaced by b_c, the half-length of the indenter/film contact area diagonal. However, because of the penetration of the film the hardness is not simply related to the load by Eq. (6b). A model proposed by Howes and Ryan (8), shown schematically in Fig. 13.10, assumes the portion of the load supported by the film is given by the film hardness, H^f, multiplied by the projected contact area on the film, $2(b^2 - c^2)$, where b and c are the half-lengths of the diagonals in the film and substrate contact zones. Similarly the portion of the load supported by the substrate is $2H^S c^2$ where H^S is the substrate hardness so that the total load is

$$P = 2H^f (b^2 - c^2) + 2H^s c^2 \tag{8}$$

Note that b and c are related via the indenter geometry and the film thickness. Measurements of P_c and b_c or c_c (the values of P, b, and c at debonding) then provide H_c^f and b_c for substitution in Eq. (5). However, if $H^f << H^s$, Eq. (8) involves determining the small difference of two large numbers and may give unreliable results. In this circumstance, it is preferable to determine H^f by direct measurement of P and c prior to penetration of the film.

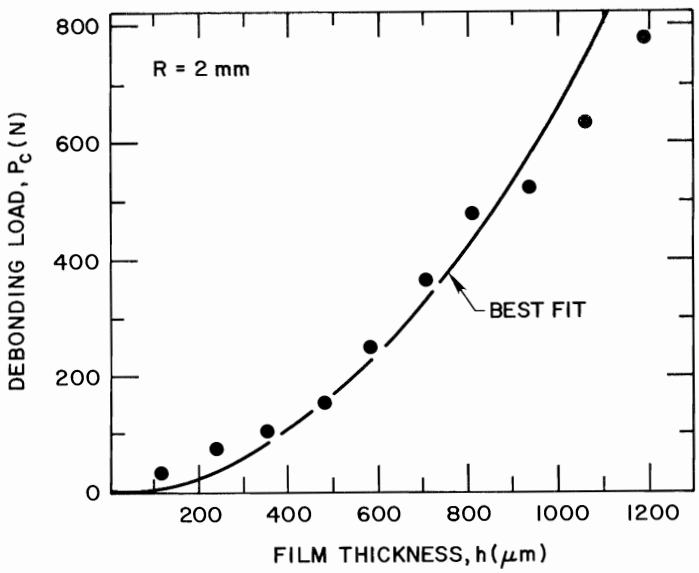

Figure 13.9: Critical load to debonding as a function of film thickness for Type II debonding of polyester films on abraded glass for a 2 mm radius spherical indenter. The best fit line is for a parabolic relationship. After Ref. 2.

13.3 THE PROPAGATION STAGE OF FAILURE

After initiation of debonding, an interfacial crack grows into a roughly circular shape until some equilibrium size is reached. Further increase in the indenter load increases the size of the crack and, in principle, the interfacial fracture resistance can be calculated from the load/crack size relationship. The situation is complex to analyze but some progress has been made. Marshall and Evans (9) have considered indentation by a Vickers pyramid which results in plastic deformation of the film (Type II initiation). They model the debonded region of the film as a clamped circular plate which has buckled away from the substrate (Fig. 13.11a). By considering changes in the elastic energy stored in the buckled plate, they determine the strain energy release rate, ζ. By assuming that the criterion for propagation of the interfacial crack is that the strain energy release rate should exceed some critical value, ζ (the usual criterion for crack growth in a homogeneous material) it may be shown that the indentation load P and crack radius c are related by

$$\frac{P^{3/4}}{c} = \text{const} \tag{9}$$

Rossington et al. (10) confirmed this relationship for ZnO films on silicon. Marshall and Evans also are able to account for residual deposition stresses in the film.

Marshall and Evans (9) draw an analogy between the debond crack and the lateral cracks that form in a homogeneous solid on **unloading** due to residual stresses around the plastically deformed zone. In other words, they assume the debond crack

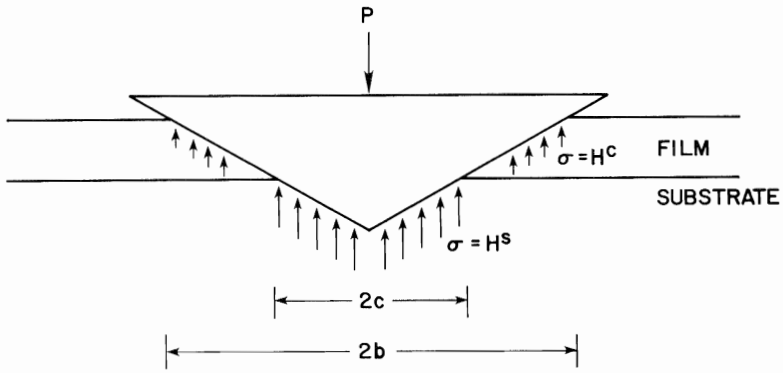

Figure 13.10: Schematic diagram of the load sharing model for Type III debonding (after Ref. 8).

forms on unloading and the buckled region of the film is not in contact with the substrate at the center of the indentation (Fig. 13.11a). In fact this analysis is not appropriate for most polymeric film systems since it is clear from the experiments of Matthewson (2) and Ritter et al. (3) that the debond crack grows while the indenter is loaded and does not grow further upon unloading. Figure 13.11b shows a more reasonable model for this situation where the buckled film is in contact with the substrate at the center of the contact. However, the buckling equations describing the film deformation for the models of Fig. 13.11 will be similar but with different boundary conditions applied at the center. Therefore, the buckling analysis of Evans and Hutchinson (11) and as used by Marshall and Evans (9) could provide a reasonable qualitative description of the debond crack in polymer films, as well as a basis for development of a more appropriate analysis.

13.4 SUMMARY

The indentation technique provides a method of determining the adhesion of polymeric films which is both simple and convenient, only requires small specimens, and which determines all important film mechanical properties in situ during the experiment. Most importantly, the technique is unique in being able to provide the interfacial shear strength and fracture resistance; both of which are required for a complete fracture mechanics description of the adhesion. However, the technique is relatively new and requires further investigation, especially in the analysis of the propagation stage.

The technique is self-consistent in that it provides adhesion estimates that do not depend on the debonding type or film thickness as exemplified by Fig. 13.12 which shows adhesion data from Ritter et al. (3) for both Type I debonding by a spherical indenter and Type II debonding by a Vickers pyramid for a range of film thicknesses. While the adhesive strength is not expected to depend on film thickness and deformation type, estimates of apparent adhesion using other test methods frequently do show

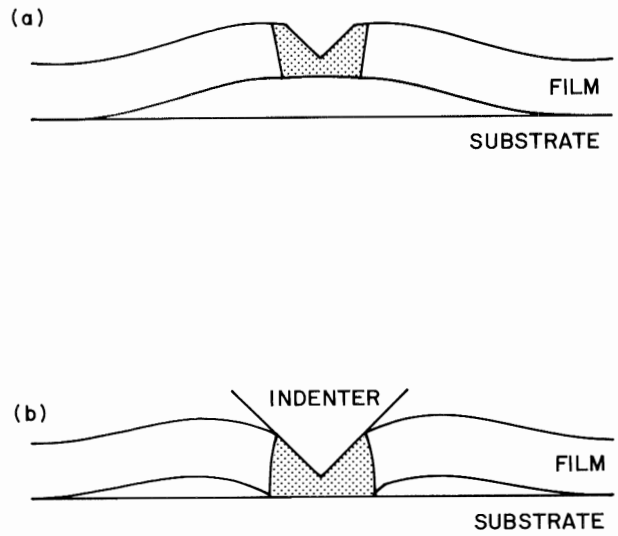

Figure 13.11: Schematic of the buckled film due to indentation induced fracture: (a) the model of Evans and Hutchinson (11) and (b) a more appropriate model for debonding of polymeric films.

dependencies on these parameters, usually due to the poor definition of the details of the debonding process.

13.5 REFERENCES

1. K. L. Mittal, "Selected Bibliography on Adhesion Measurement of Films and Coatings," *J. Adhesion Sci. Tech.*, 1, 247 (1987).
2. M. J. Matthewson, "Adhesion Measurement of Thin Films by Indentation," *Appl. Phys. Lett.*, 49, 1426 (1986).
3. J. E. Ritter, T. J. Lardner, L. Rosenfeld, and M. R. Lin, "Measurement of Adhesion of Thin Polymer Coatings by Indentation," *J. Appl. Phys.*, in press (1989).
4. M. W. Vratsanos, E. L. Thomas, and R. J. Farris, "The Adhesive Behavior of Poly(p-phenylene benzobisthiazole) (PBT)/epoxy Composites," *J. Mat. Sci.*, 22, 419 (1987).
5. K. L. Johnson, **Contact Mechanics,**, 136, Cambridge University Press, Cambridge, U.K., (1985).
6. M. J. Matthewson, "Axi-symmetric Contact on Thin Compliant Coatings," *J. Mech. Phys. Solids*, 29, 89 (1981).
7. D. M. Marsh, "Plastic Flow in Glass," *Proc. Roy. Soc.*, A279, 420 (1964).
8. V. R. Howes and M. A. Ryan, "The Effect of Protective Coatings on Indentation Phenomena for Glass," *J. Aust. Ceram. Soc.*, 22, 13 (1986).

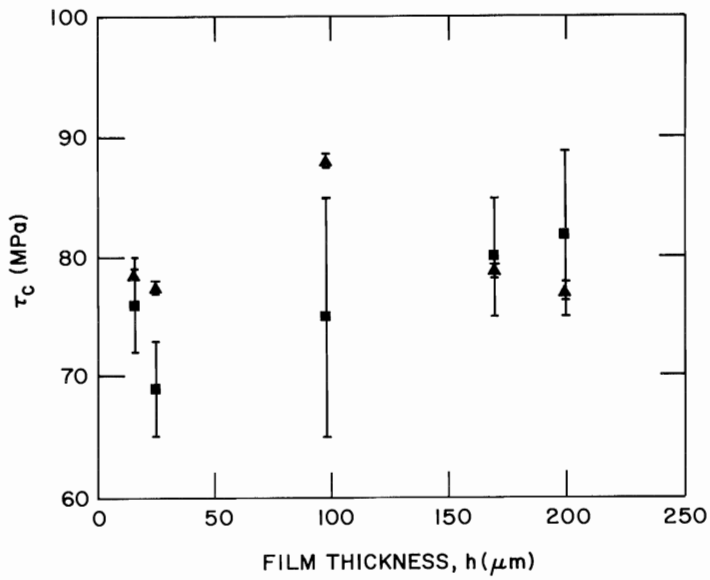

Figure 13.12: Adhesive shear strength measurements on epoxy films of various thicknesses using (■) a 2-mm-radius ball indenter (Type I debonding) and (▲) a Vickers indenter (Type II debonding). After Ref. 3.

9. D. B. Marshall, and A. G. Evans, "Measurement of Adherence of Residually Stressed Thin Films by Indentation. I. Mechanics of Interface Delamination," *J. Appl. Phys.*, 56, 2632 (1984).

10. C. Rossington, A. G. Evans, D. B. Marshall, and B. T. Khuri-Yakib, "Measurements of Adherence of Residually Stressed Thin Films by Indentation. II. Experiments with ZnO/Si," *J. Appl. Phys.*, 56, 2639 (1984).

11. A. G. Evans and J. W. Hutchinson, "On the Mechanics of Delamination and Spalling in Compressed Films," *J. Solids Structures*, 20, 455 (1984).